Behaviour of Stainless Steel Beam-to Column Joints-
Part 2: Numerical Modelling and Design Recommendations

Mohamed Elfla, Marios Theofanous & Samir Dirar

University of Birmingham, Dept. Civil Engineering, UK

Abstract

Following the six full-scale tests reported in the companion paper, this paper reports a detailed numerical (FE) study on planar stainless steel beam-to-column joints. An FE model is developed and validated against the obtained experimental results, and parametric studies are conducted to obtain the moment-rotation characteristics of a wide range of beam-to-column joints classified as semi-rigid and/or partial strength. The design rules for stainless steel connections, which are based on the specifications of EN 1993-1-8 for carbon steel joints, are reviewed and are found to be overly conservative in terms of strength and inaccurate in terms of stiffness thus necessitating the development of novel design guidance in line with the observed structural response.

Keywords

Stainless steel joints, beam-to-column joints, Eurocode 3, Numerical modelling, Semi-rigid connections, design recommendations

1 Introduction

In the companion paper [1] the authors have reported six full scale tests on single-sided stainless steel beam-to-column joints. Full details of the tests including general setup and instrumentation, obtained moment-rotation response, initial stiffness, ultimate moment resistance, failure modes and material response of the joint components have been disclosed. Based on the obtained results, the design provisions of EN 1993-1-8 [2], which are assumed to be applicable for both carbon steel and stainless steel [3], were found to consistently underestimate the plastic moment resistance and overestimate the joint initial rotational stiffness.

This paper complements the companion paper [1] by investigating numerically the response of single-sided stainless steel beam-to-column joints under monotonic loads. The models were shown capable to accurately replicate the response of the tested joints in terms of initial stiffness, ultimate moment resistance, failure modes and overall moment-rotation response. Upon validation, the FE models were used to conduct parametric studies on joint typologies similar to the ones adopted in the experimental part of the research [1], namely flush end plate (FEP), extended end plate (EEP), top and seat angle cleat (TSAC) and top, seat and web angle cleat (TSWAC). The investigated parameters included bolt end and edge distances, angle cleat and end plate thickness, column flange thickness and material grade of the connected members. A total of 132 parametric studies have been performed thus providing a comprehensive database of validated FE results on the response of stainless steel joints over a wide range of structural configurations likely to be employed in practice resulting in a variety of failure modes. The generated numerical data are used to assess the applicability of the design provisions of EN1993-1-8 [2] and to generate novel design recommendations.

2 Numerical Modelling

Three dimensional finite element models of the joints studied experimentally in the companion paper [1] were developed using the general purpose FE software ABAQUS [4] and details of the modelling procedure are reported herein. The geometry of the simulated joints, against which the models were validated are shown in Fig. 1, where the symbols adopted in parametric study reported in this paper are also defined. The values of the geometric dimensions defined in Fig. 1 are given in Table 1 for the tested specimens.

2.1 Development of FE models

The components of the connections that were explicitly simulated include the connected beam and column, the bolts, the end plate and the angle cleats. The welds between the beams and the end plates were not explicitly modelled, since their response is rigid (i.e. welds can be assumed to have infinite stiffness) and no weld failure occurred during testing. Instead, a tie constrain was defined to tie the degrees of freedom of the nodes of adjacent surfaces that were welded thus preventing separation and overlapping of the respective elements. A further simplification of the simulated geometry included ignoring the threaded geometry of the bolt shank and modelling it as a smooth cylindrical surface with a diameter such that the area of the modelled bolts equals the stress area of the real bolts. Furthermore, the bolt head, bolt nut and washers were simplified as cylinders which were tied to the bolt shank. The boundary conditions employed in the FE models simulated the ones applied in the experimental study. Hence all degrees of freedom of the bottom end cross-section of the column were restrained, whilst the horizontal translation of the top end of the column in the plane of

Paper presented by Marios Theofanous - m.theofanous@bham.ac.uk

loading was also restrained. The loaded end of the beam was loaded by incrementally applying a downward displacement, whilst out of plane translations were restrained.

All modelled components were discretized with the eight-noded (hexaedron) 3D solid first-order reduced integration element C3D8R. Several mesh densities were considered and a structured mesh was employed. The components of the connection subjected to sharp stress gradients, such as the end plates, angle cleats and bolts, as well as the parts of the beam and the column in the vicinity of the bolt holes were discretised with a fine mesh, whilst a coarser mesh was used for the discretisation of parts of the beam and the column far from the joint region, the response of which was predominantly elastic. At least three elements were provided through the thickness of thin-walled components such as end plates, angle cleats, flanges and webs to accurately capture their out-of-plane flexure and avoid the effect of shear locking. The employed mesh density is depicted in Figs.2-4, where the numerically obtained failure modes are compared to the experimental ones.

The contact between the various non-welded components of each joint was modelled by using the "surface to surface" contact algorithm provided by ABAQUS. Surfaces discretised with course meshes were selected as master surfaces, whilst the more finely discretised surfaces were selected for salve surfaces. The contact pressure-clearance relationship was defined as "hard contact" for all cases to allow full transfer of the compression loads and separation after contact. The penalty method with a friction coefficient of 0.3 was defined for the tangential response of all contact surfaces. Small sliding contact formulation was used at the interface between angle cleats and bolt heads, end plates and bolt heads and the seat angle cleat and the column/beam flange. Finite sliding contact formulation was employed for all other contact pairs (e.g. bolt shank and clearance hole), thus allowing for large slip.

Material nonlinearity was considered using the von Mises yield criterion coupled with isotropic hardening; hence the yield surface was assumed to expand uniformly in the stress space with increasing plastic strains. The Young's modulus values characterising the elastic material response and the stress-strain values used to define the plasticity model were derived from the experimental tests reported in the companion paper [1]. Since large plastic strains developed in all joints, analytical material modelling capable of approximating the material response throughout the full strain range was required. To this end the two-stage Ramberg-Osgood material model [5, 6] was adopted. This model adopts the original Ramberg-Osgood model for stresses lower than the 0.2% proof stress and employs a similar curve thereafter until the ultimate tensile stress. The two-stage Ramberg-Osgood model was chosen over its three-stage variant [7], because it is adopted by EN1993-1-4 [3]. The relevant material parameters for the analytical approximation of the material response as determined from tensile coupon testing [1] are reported in Table 2, where the plastic strain at fracture is also reported and n and m are strain-hardening exponents used in the two-stage Ramberg-Osgood model. The stress and strain values obtained through analytical modelling were converted into the true stress and logarithmic plastic strain format as required by ABAQUS.

Bolt fracture occurred during testing and ultimately triggered the failure of the joints [1], hence failure of the bolts has to be accounted for in the numerical models. In ABAQUS material fracture and failure can be explicitly defined for metals by defining appropriate damage initiation and damage evolution criteria, which simulates the ductile fracture of metals via void nucleation and growth [4]. However, in the absence of relevant material parameters a simplified approach was followed, according to which fracture of the components was not explicitly modelled, but was indirectly defined on the basis of the uniaxial plastic strain at fracture ε_f, which is reported in Table 2 for all components comprising the tested joints. Hence bolts were assumed to fail when their equivalent plastic strain obtained from the analysis reached the respective plastic strain at fracture ε_f given in Table 2 throughout any element in the bolt shank. A similar approach of indirectly defining fracture via ε_f was successfully followed in [8], where the net section failure of stainless steel bolted connections was simulated. It should be noted that in cases where the bolts were primarily loaded in tension or tension and shear, strain localisation (i.e. necking) occurred during the analysis prior to reaching the equivalent plastic strain of the bolts. Similar observations regarding the ability of FE models to reproduce ultimate deformation patterns of steel in tension based on geometric instabilities alone (i.e. without utilising material instability approaches) have previously been made for steel tensile specimens [9].

The complex contact conditions between the various interacting parts comprising each joint led to convergence difficulties. These were overcome by employing a quasi-static explicit dynamic analysis procedure using the ABAQUS/EXPLICIT solver [4], which is well suited for highly nonlinear problems. Explicit dynamic analysis usually requires the execution of tens of thousands of computationally inexpensive increments, during which the solution is propagated form the previous step, thus avoiding convergence issues. Mass scaling was utilised to reduce computational time, whilst quasi-static response was achieved by specifying a slow displacement rate and checking that the kinetic energy was smaller than 2% of the internal energy for the greatest part of the analysis, thus ensuring that inertia effects were insignificant.

2.2 Validation

The numerical models were validated against the experimental results reported in [1]. Fig. 2 displays the experimental and numerical failure modes for FEP and EEP joints at the deformation corresponding to the maximum load. Both the test specimen and the numerical model display large inelastic deformations of similar magnitude in the column flange and the end plates. Moreover, the numerical model accurately predicted necking of the bolts in the top bolt row of FEP, which indicates bolt fracture, as shown in Fig. 2 (a). The bolt plastic deformation shown in Fig. 2(b) is similar for both the experimental and the numerical failure modes. The accuracy of the FE models for FEP and EEP joint is

demonstrated in Fig. 3, where the experimental and numerical moment-rotation response is depicted. The numerical curves accord well with the experimental ones throughout the full range of the curves.

The experimental and numerical failure modes and corresponding experimental and numerical moment-rotation curves are depicted for both TSAC and TSWAC joints in Figs. 4 and 5 respectively. Once again an excellent agreement between the experimental and numerical results can be observed in terms of failure modes and overall moment rotation response. The numerical curve for TSWAC-10 depicted in Fig. 4(b) is plotted with a bold line until the equivalent plastic strain of the bolt reaches its limiting values, and with a dotted line thereafter. Hence it can be observed that the FE prediction for bolt failure coincides with the experimentally observed failure thus demonstrating the appropriateness of defining bolt fracture on the basis of the plastic strain at fracture ε_f.

The accuracy of the numerical models is quantified and assessed in terms of the initial rotational stiffness $S_{j,ini}$, the plastic moment resistance $M_{j,R}$, the ultimate moment resistance $M_{j,max}$ and the rotation corresponding to $M_{j,max}$ $\Phi_{j,u}$ in Table 3, where the ratio of the numerical predictions over the respective experimental values is reported. Overall, an excellent agreement between the numerical and experimental results can be observed for all joints in terms of the plastic moment resistance $M_{j,R}$ and a good agreement is obtained for the ultimate moment resistance $M_{j,max}$ and corresponding rotation $\Phi_{j,u}$, bearing in mind that these quantities are neither quantified in [2] nor explicitly used in design, but nonetheless can be utilised to assess the available ductility of the connections. The stiffness is less well predicted predominantly due to poor predictions for the TSAC joints and is predicted with reasonable accuracy for the end plate specimens (both FEP and EEP) and the TSWAC specimens. The observed discrepancies in the prediction of the stiffness are arguably attributable to the gaps and slips between the various bolted components of non-preloaded bolted connections, which cannot be easily quantified or accounted for neither in numerical modelling nor in design standards. Given that the initial stiffness of stainless steel joints will be no different from that of carbon steel joints and that the overall connection response and failure modes are reasonably well predicted, parametric studies are conducted hereafter to generate numerical data on the basis of which the design provisions of [2], particularly the plastic moment resistance $M_{j,R}$ can be assessed.

3 Parametric Studies

Upon validation of the FE models parametric studies were performed to enable the study of the behaviour of stainless steel connections over a wide range of geometric configurations and highlight the influence of key joint details on the overall response. The four joint typologies against which the FE models were calibrated, namely FEP, EEP, TSAC and TSWAC, are employed in the parametric studies. Moreover, the response of geometrically identical joints made in Grade EN 1.4162 (lean duplex) stainless steel is investigated. The lean duplex stainless steel grade was chosen as a representative duplex grade which displays higher strength and lower ductility than the austenitic grade. The material parameters used for the lean duplex material were taken from [10]. Hence two series of geometrically identical models were considered, one simulating the response of austenitic stainless steel and one simulating the response of lean duplex stainless steel joints, which are denoted by the letters A and L following the joint designation respectively (e.g. EEP-A is an extended end plate joint in austenitic stainless steel). All relevant symbols of the varied geometric dimensions are defined in Fig. 1.

The parameters varied for the parametric studies of joints FEP-A and FEP-L include the thickness of the column flange t_f, the thickness of the end plate t_p, the edge distance of the bolt rows from the end plate edges/column edges e_1 and the distance of the top bolt row from the centroid of the compression beam flange z as reported in Tables 4 and 5. Similarly, the geometric parameters varied for the EEP-A and EEP-L joints are defined in Tables 6 and 7. With respect to the TSAC specimens Tables 8 and 9 define the investigated parameters, which include the column flange thickness t_c, the angle cleat thickness t_a (both top and seat cleats were assumed to have the same geometric dimensions), the edge distance e_1 of the bolts connecting the top cleat to the column flange, the depth L_1 of the leg of the cleats parallel to the column flange and the gap g between the beam and the column flange. Similar parameters were considered for the TSWAC-A and TSWAC-L joints, the web cleat of which was kept unchanged, as shown in Tables 10 and 11. In this case the edge distance e_1 of the bolts connecting the top angle cleat to the column flange were kept constant, whilst the edge distance e_2 of the bolts connecting the web cleats to the column flange were varied.

Similar to the experimental tests, the FE models exhibited large plastic deformations in the stainless steel components (i.e. column flange, end plates and angle cleats) with increasing loading prior to reaching the joints' ultimate failure moment. In all cases joint failure was triggered by bolt failure, since the bolts possess markedly reduced ductility compared to the other joint components as indicated by their significantly lower plastic strain at fracture ε_f. In order to characterise the observed yield line patterns occurring prior to the attainment of the ultimate moment resistance, the end plates and angle cleats have been divided in discrete yield zones, which are defined in Fig. 6. Fig. 7 depicts the evolution of the equivalent plastic strains in the yield zones of joint components and the corresponding development of yield line patterns for typical joint models. The yield zone exhibiting the largest plastic strains compared to the other zones is reported in Tables 5-11 for each joint model and characterises the overall joint response prior to failure. In addition to the geometric configurations and the yield zone governing the yield line patterns of the modelled joints, the numerical results for $S_{j,ini}$, $M_{j,R}$, $M_{j,max}$ and $\Phi_{j,u}$ and the corresponding predictions of EN 1993-1-8 [2] for $S_{j,ini}$ and $M_{j,ini}$ are also reported in Tables 4-11 and are discussed in the following section.

4 Results and Discussion

4.1 Flush end plate (FEP) connections

The geometry of the simulated joints and the obtained results are reported in Tables 4 and 5 for the models employing austenitic (FEP-A) and lean duplex (FEP-L) material properties respectively. Fig. 8 depicts the obtained moment-rotation (M-Φ) curves of the modelled FEP-A joints for different end plate thicknesses t_p (Fig. 8 (a)), edge plate distances e_1 (Fig. 8(b)), column flange thicknesses t_f (Fig. 8 (c)) and distances of the top bolt row from the centroid of the compression beam flange z (Fig. 8(d)). As expected, increasing the lever arm z, or decreasing the edge distance e_1, leads to a marked increase of both the strength and the stiffness of the connections. Moreover, increasing z, seems to change the predominant yield zone from 3 (end plate in the vicinity of the welded beam web) to 1 (end plate in the vicinity of the flange). Increasing the end plate thickness t_p also increases the strength and the stiffness of the FEP-A joints by increasing the resistance of the equivalent T-stub [11]. However, the effect is less pronounced as increasing the end plate thickness beyond a certain value (beyond 12 mm for the parameter range considered herein, as shown in Fig. 8(a)), shifts the failure mode to the column flange, which becomes the weakest component of the connection. Similarly, increasing the column flange thickness t_f beyond 12 mm has a limited effect on the strength and stiffness as the end plate is already the weakest component of the joint, whilst decreasing it more drastically affects the joint response, by shifting the failure mode from "end plate in bending" to "column flange in bending". In all cases, an increase in strength is accompanied by a corresponding decrease in the rotation at which the ultimate moment occurs.

Similar observations can be made for the lean duplex models FEP-L, the response of which is shown in Fig. 9. Comparing the response of the models with different materials, it can be concluded that the lean duplex joints exhibit higher strength but lower ductility compared to their austenitic stainless steel counterparts. This can be attributed to the increased strength of the various components due to the higher material proof stresses. Since lean duplex stainless steel reaches higher stresses at lower strains compared to austenitic stainless steel, the rotation at which the bolt force capacity is reached decreases, hence, bolt failure and overall joint failure is triggered at smaller rotations. Similar observations were made in [12], where geometrically identical T-stubs were experimentally verified to have higher resistance and lower deformation capacity for higher steel grades.

4.2 Extended end plate (EEP) connections

The geometry of the simulated joints and the obtained results are reported in Tables 6 and 7 for the models employing austenitic (EEP-A) and lean duplex (EEP-L) material properties respectively. Figs. 10 and 11 display the M-Φ response of the modelled joints for various geometric configurations. In general, the same remarks made for the FEP connections apply, as increasing the plate thickness, decreasing the edge distance and increasing bolt distance from the compression flange of the beam lead to enhanced strength and stiffness but reduced ductility, whilst the effect of the flange thickness is less pronounced. Moreover, the lean duplex stainless steel joints (EEP-L) display higher strength but lower ductility compared to geometrically identical joint in austenitic stainless steel (EEP-A) as previously discussed.

4.3 Top and seat angle cleat (TSAC) connections

The geometry of the simulated joints and the obtained results are reported in Tables 8 and 9 for the models employing austenitic (TSAC-A) and lean duplex (TSAC-L) material properties respectively. Fig. 12 depicts the effect of the investigated parameters on the joint M-Φ response. From Fig. 12 (a) it can be observed that increasing the angle thickness significantly enhances both the strength and the stiffness of the TSAC joints, but leads to a drop in the rotation at ultimate moment $\Phi_{j,u}$, since the thicker and hence stiffer angles transfer a higher tensile force and cause bolt failure at smaller deformations compared to the thin ones. This can be clearly observed in Fig. 13, where the failure modes of two TSAC joints with different angle thicknesses are shown. Both joints ultimately fail by tensile fracture of the bolts connecting the top angle cleat to the column face. However, the joint with the thicker angle cleat transmits high tensile forces to the top bolts at relatively small rotations, whereas the thinner angle cleat (t_a=8 mm) undergoes significant inelastic bending of the top angle cleat, which is almost flattened prior to causing bolt fracture. The effect of flattening due to large inelastic bending of the top cleat is shown in the lower curve of Fig. 12 (a), where an increase of the joint stiffness can be observed at large rotations, arguably due to the angle cleat transmitting forces primarily in tension instead of bending. Similarly to the angle cleat thickness, the length L_1 of the angle cleat leg parallel to the column flange also has a marked effect on the response, with increasing leg lengths leading to smaller angle cleat resistances and hence smaller moment capacities and more flexible response.

On the other hand changing the column flange thickness t_f does not have any noticeable effect on the joint response as shown in Fig. 12(c), since the column flange remains significantly stiffer and stronger than the angle cleat for the range of parameters considered. Similarly the effect of bolt edge distance e_1 (Fig. 12(d)) is negligible since, contrary to the end plate connections, the edge distance does not affect the effective leg of the equivalent T-stub, which is in agreement with the design provisions of EN 1993-1-8[2]. Finally the effect of the gap g between the beam and the column does not seem to have significant influence on the joint response for the range of parameters considered, with decreasing gap leading to slightly stiffer response. This is because in all cases considered herein, bending of the top cleat dominates the response. Similar observations can be made for TSAC-L joints, as shown in Fig. 14. As before, the increase in the nominal yield strength leads to higher moments and stiffer response but reduced ductility.

4.4 Top, seat and web cleat connections

In Tables 10 and 11 the results of the parametric study for TSWAC-A and TSWAC-L are reported, whilst Fig. 15 shows the effect of varying geometric parameters on the joint response. The comments regarding the effects of the angle cleat thickness t_a and the angle cleat leg L_1 on the joint response made for the TSAC joints are valid for the TSWAC joints. Given that e_1 did not seem to have any effect on the behaviour of the TSAC joints this parameter was not considered for TSWAC joints and the edge distance e_2 of the bolts connecting the web cleats to the column flange was varied instead. Due to the presence of the web cleats higher moment and an overall stiffer response is obtained. Moreover, the behaviour of the connection is no longer dominated by the top cleat response, which leads to non-negligible effects of changing the edge distance e_2 of and flange thickness t_f, since flexure of the column flange occurs for this joint configuration contrary to the TSAC specimens, where almost all of the plastic deformations were localised in the top angle cleat. The effect of the bending of the column flange can be deduced by observing the failure modes shown in Figs.13 and 16(a) for a TSAC and TSWAC configuration respectively. In Fig. 13, the column flange remains almost unreformed as the top angle cleat is significantly weaker and hence attracts all the plastic deformation, whereas some flexure of the column flange can be seen in Fig. 16(a). Therefore increasing the flange thickness or reducing the bolt edge distance e_2 leads to an increased strength and stiffness.

Contrary to the TSAC specimens, the gap g between the beam and the column was observed in this case to have a very strong influence on the joint ultimate moment, ductility and failure mode. When there is no gap between the beam and the columns, compression is transmitted from the beam bottom flange to the column via contact, whereas by shifting the beam away from the column, shear forces are developing on the bolts connecting the beam bottom flanges to the seat angle cleats. This has a small effect on the joint stiffness but a marked effect on the observed failure mode as shown in Fig. 16, where the deformed shape at failure of a TSWAC joint without gap (g=0) and a TSWAC joint with a 9 mm gap (g=9 mm) is depicted. In the latter case significant shear stresses are acting on the bolts connecting the seat cleat to the beam bottom flange, which may fail in single shear prior to tensile fracture of the bolts connecting the top and web cleats to the column flange, as clearly shown in Fig. 16(c). Premature bolt failure leads to a reduced strength and stiffness with increasing gap distance g.

4.5 Assessment of design provisions

In Tables 4-11 the average value and coefficient of variation of the EN 1993-1-8 [2] predictions over the numerical ones in terms of initial rotational stiffness $S_{j,ini}$ and plastic moment resistance $M_{j,R}$ is given. The stiffness is consistently over-predicted by about 50% for FEP and EEP joints for both stainless steel grades considered whilst for TSAC and TSWAC joints the over-predictions are even more severe. These findings are in agreement with similar conclusions on the accuracy of the stiffness predictions of [2] as discussed in [1] and relate predominantly to uncertainties regarding tolerances and contact between the various components inherent in non-preloaded bolted connections.

In terms of the plastic moment resistance, in all cases the Eurocode model yields significantly conservative results. The ratio of the codified over the numerical moment resistance of the FEP-A and EEP-A joints is 0.45 and 0.61 respectively, whilst the corresponding values for the FEP-L and EEP-L joints are 0.51 and 0.65. In all cases the coefficient of variation is reasonably small (ranging from 0.06 to 0.09), thus indicating constituently conservative design predictions. With regard to the TSAC-A and TSAC-L joints the respective values are 0.55 and 0.63 with coefficients of variation equal to 0.09 and 0.11 respectively. Finally the moment resistance of the TSWAC joints is also under-predicted (0.61 for TSWAC-A and 0.85 for TSWAC-L) respectively, however the scatter of the predictions is in this case higher (0.15 and 0.19 respectively). Overall it can be observed that the conservatism is higher for austenitic stainless steel joints compared to their lean duplex counterparts. This is due to the higher ductility and strain hardening characteristics of the austenitic stainless steels. Moreover, the conservatism seems to be higher for joints exhibiting more ductile behaviour (higher rotation values at failure) compared to joints failing at smaller rotations (e.g. TSWAC-L). These observations agree well with the ones based on the test results alone [1].

The significant strain-hardening exhibited by stainless steels has been shown to lead to higher cross-section capacities compared to the codified ones [13] for stocky stainless steel cross-sections, which can reach stresses higher than the nominal yield stress if they do not buckle locally. This is more pronounced in the case of connections, provided that their response is governed by a ductile failure mode such as bending of the end plate, angle cleat or column flange, since the critical components are either in bending or in tension and hence only material ductility limits the level of strain-hardening that can be attained. Based on the above observations the development of a design model in agreement with the observed structural response is warranted. The development of a component based design model employing nonlinear springs is currently under way at the University of Birmingham. The model utilises the continuous strength method framework for the determination of the moment resistances of the idealised T-stubs and initial results are promising.

5 Conclusions

A numerical model has been developed and validated against the experimental data reported in the companion paper [1]. A comprehensive parametric study was conducted and the structural response of 132 joints has been obtained numerically. Based on the numerical results the effect of key geometric parameters on the joint response has been investigated and the design provisions codified in EN1993-1-8 [2] were assessed. The effect of the adopted stainless steel grade on the joint response has also been studied and it was established that lean duplex stainless steel joints exhibit

higher strength but lower ductility than geometrically identical austenitic joints. The plastic moment resistance was found to be underestimated by 44% and 34% on average for austenitic and lean duplex stainless steel joints. The development of a design method in line with the observed structural response is warranted.

In addition to the conservatism exhibited by EN 1993-1-8, the both the experimental [1] and the FE study have demonstrated that stainless steel joints exhibit high ultimate moment resistances and excellent ductility. Even though such high rotations and moment resistances cannot be practically utilised in conventional design scenarios, the high ductility and moment resistances of stainless steel components can arguably accommodate the significant ductility demands imposed by accidental actions such as a column loss scenario [14].

Acknowledgements

The financial support received from the Libyan government by the first author is gratefully acknowledged. The authors would like to thank Mr David Price, laboratory technician in the Department of Metallurgy and Materials for his assistance with the material coupon tests.

References

[1] Elflah M., Theofanous M., Dirar S. Behaviour of stainless steel beam-to-column joints - Part 1: experimental investigation.(submitted 5th Itnernational stainless steel experts seminar)

[2] EN 1993-1-8. Eurocode 3: Design of steel structures – Part 1-8: Design of joints., British Standards Institution, CEN, 2005.

[3] EN 1993-1-4+A1, Eurocode 3: Design of steel structures - Part 1.4: General rules Supplementary rules for stainless steel, CEN, 2015.

[4] ABAQUS (2013) Theory Manual, ver 6.13,Dassault Systèmes Simulia Corp Providence, RI, USA.

[5] Mirambell, E., Real, E. (2000). On the calculation of deflections in structural stainless steel beams: an experimental and numerical investigation. Journal of Constructional Steel Research. 54(1), 109-133.

[6] Rasmussen KJR. Full-range stress–strain curves for stainless steel alloys. J Constr Steel Res 2003;59(1):47-61.

[7] Quach WM, Teng JG, Chung KF. Three-stage full-range stress–strain model for stainless steels. J Struct Eng ASCE 2008;134(9):1518-27.

[8] Salih E.H, Gardner L., Nethercot D.A. Numerical investigation of net section failure in stainless steel bolted connections, Journal of Constructional Steel Research 66(12):1455-1466, 2010.

[9] Okazawa S., Usami T., Noguchi H., Fujii F. Three-Dimensional Necking Bifurcation in Tensile Steel Specimens. J of Engineering Mechanics 128(4): 479-486, 2002.

[10] Cross-section stability of lean duplex stainless steel welded I-sections. Journal of Constructional Steel Research, 80: 1-14.

[11] P. Zoetemeijer, A design method for the tension side of statically loaded, bolted beam-to-column connections, HERON 20 (1), 1974.

[12] Girao Coelho, A.M., Bijlaard, F.S.K., Gresnigt, N., da Silva, L.S. Experimental assessment of the behaviour of bolted T-stub connections made up of welded plates. Journal of Constructional Steel Research 60(2): 269-311, 2004.

[13] Gardner L., Theofanous M. Discrete and continuous treatment of local buckling in stainless steel elements, Journal of Constructional Steel Research 64(11):1207-1216, 2008.

[14] Byfield M., Mudalige W., Morison C., Stoddart E. A review of Progressive Collapse research and regulations. Proceedings of the Institution of Civil Engineers: Structures and Buildings 167(8): 447-456, 2007.

6 Figures

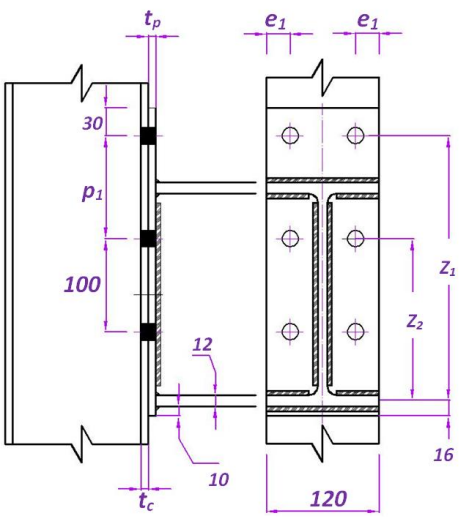

(a) Extended End Plate (EEP) connection

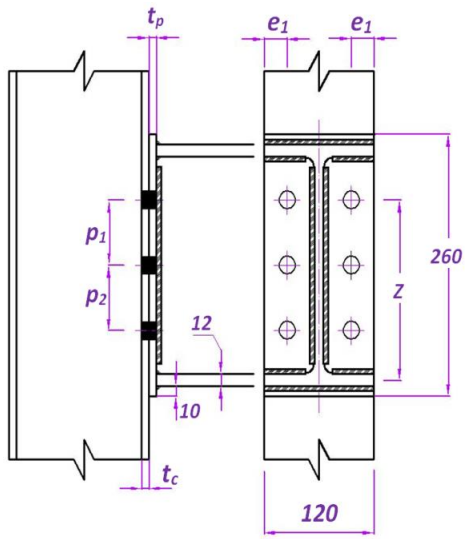

(b) Flush End Plate (FEP) connection

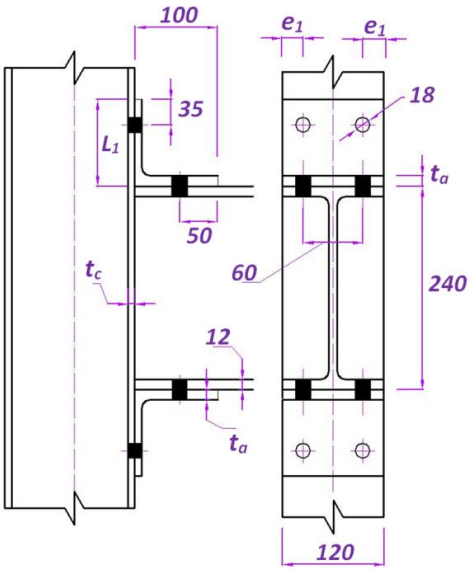

(c) Top and Seat Angle Cleat connection (TSAC)

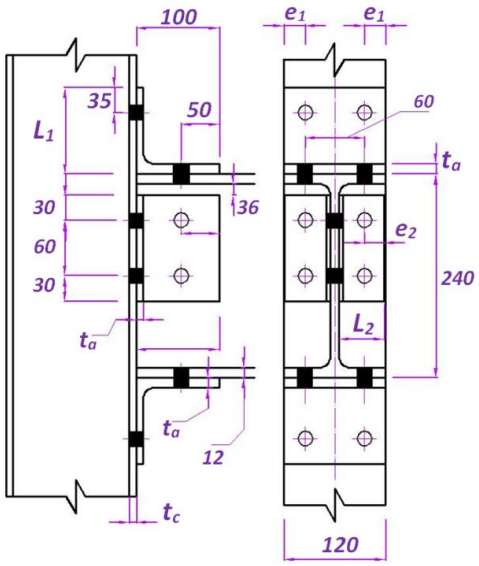

(d) Top, Seat and double Web Cleat (TSWAC) connection

Fig. 1 Joint details of the tested specimens (see Table 1 for dimensions corresponding to the symbols)

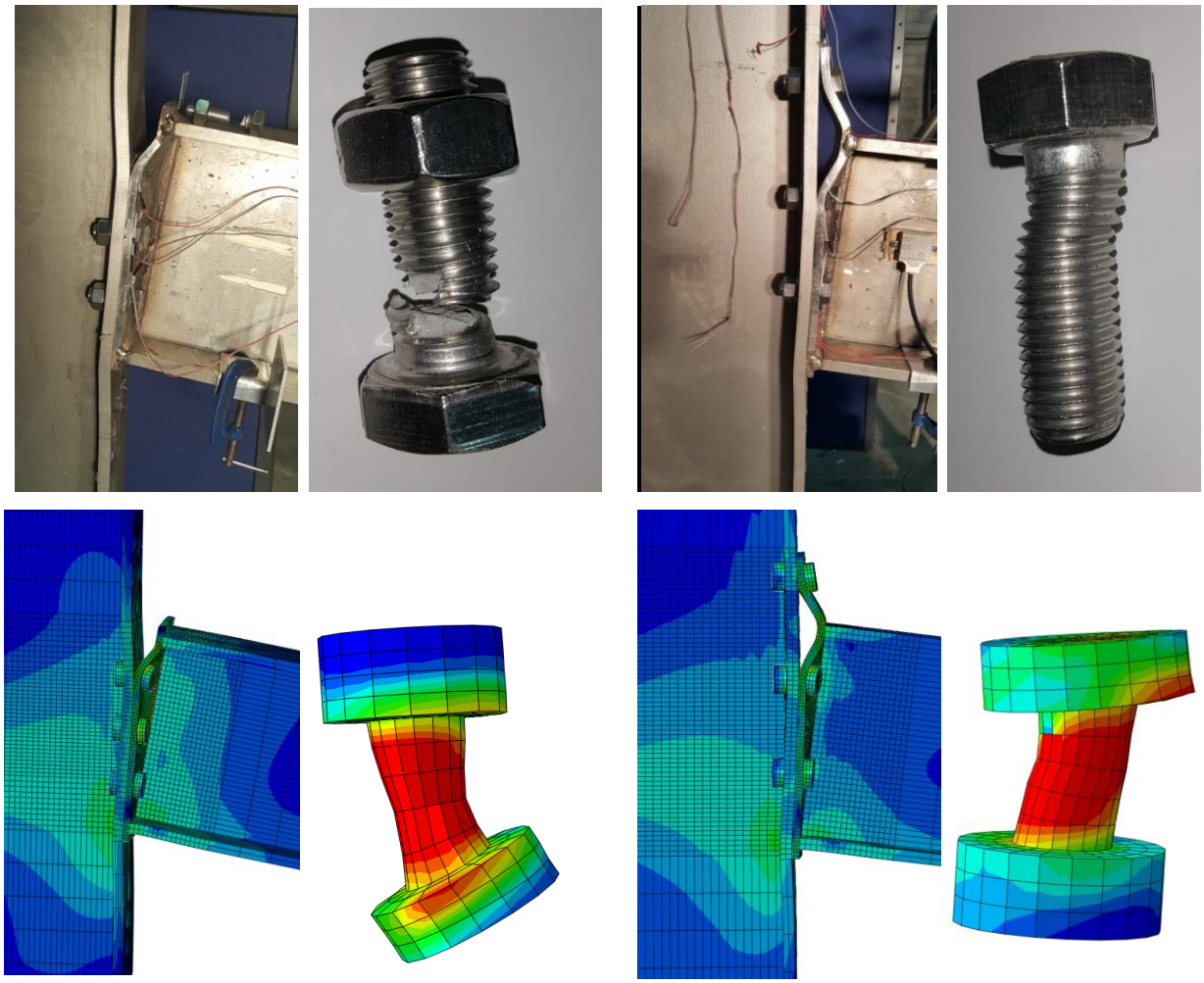

(a) Flush End Plate (FEP) connection failure mode and fractured top bolt

(b) Extended End Plate (EEP) connection failure mode and deformed top bolt

Fig. 2 Experimental and numerical failure modes of FEP and EEP joints and close-up of bolt at failure

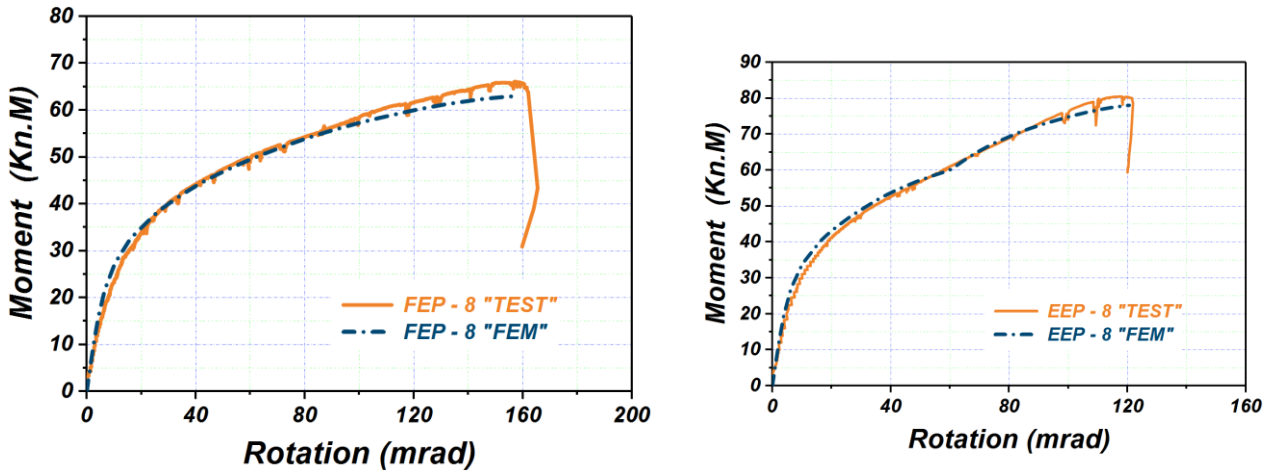

a) FEP

b) EEP

Fig. 3 Experimental and numerical moment-rotation response for: (a) FEP ad (b) EEP.

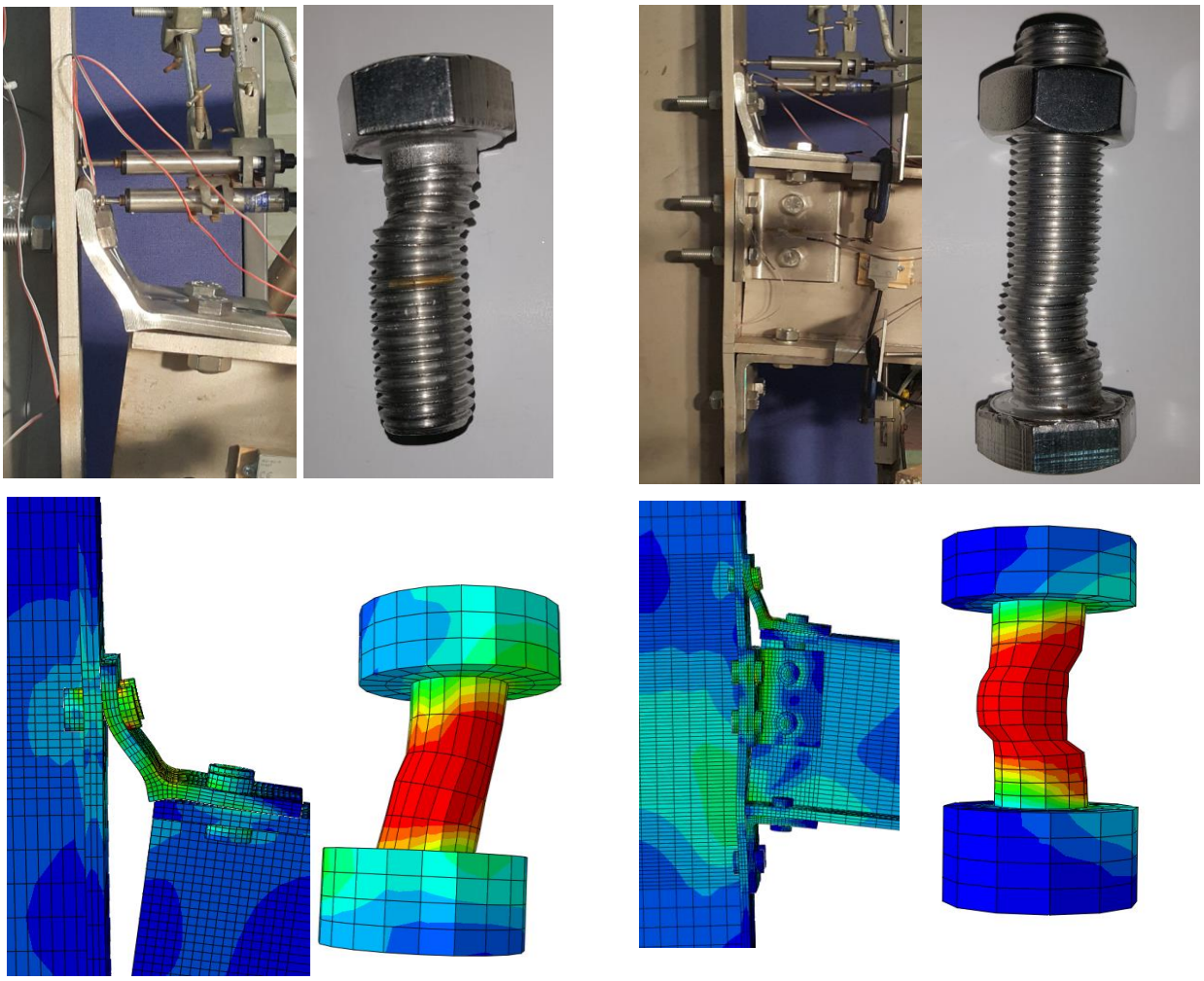

(a) Top and Seat Angle Cleat (TSAC-10) connection failure mode and bolt failure in tension and shear

(b) Top, Seat and Web Angle Cleat (TSWAC-10) connection failure mode and bolt failure in double shear

Fig. 4 Experimental and numerical failure modes for (a) TSAC-10 and (b) TSWAC-10 joints and close-up of bolt corresponding bolt failures

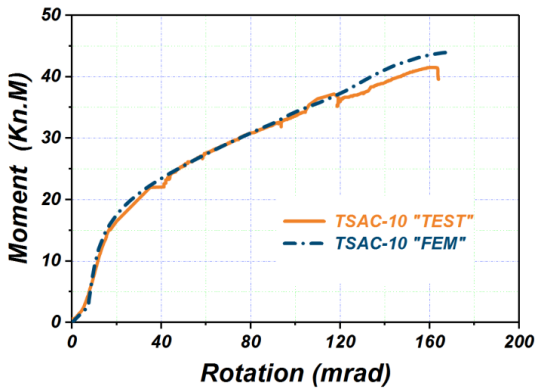

a) TSAC-10

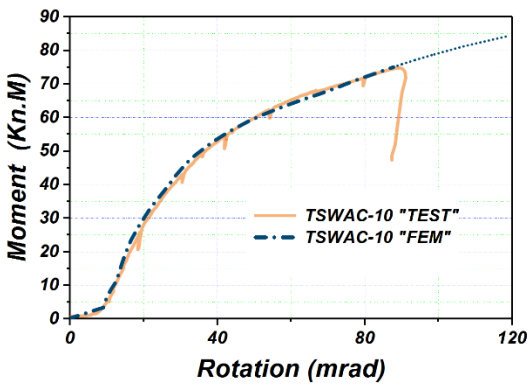

b) TSWAC-10

Fig. 5 Experimental and numerical moment rotation response for: (a) TSAC-10 ad (b) TSWAC-10.

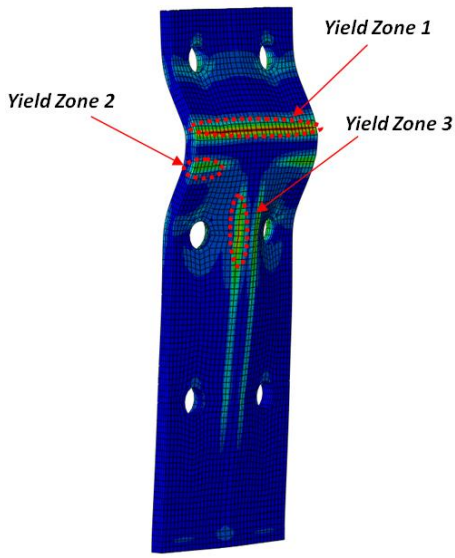

a) FEP

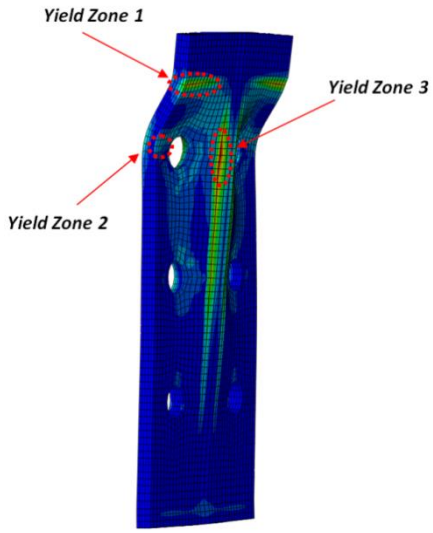

b) EEP

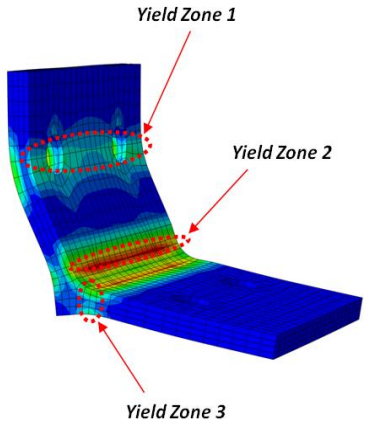

c) TSAC

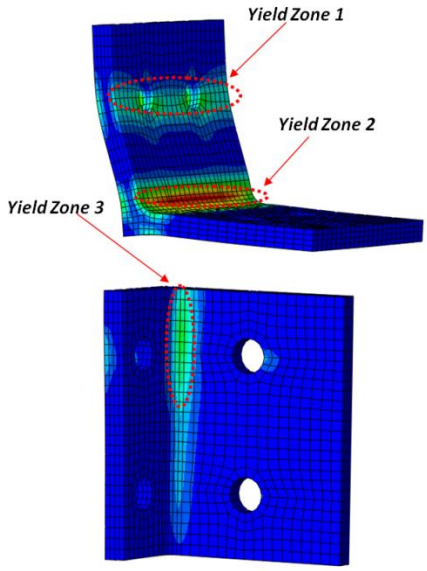

d) TSWAC

Fig. 6 Definition of yield line zone patterns for end plates and angle cleats

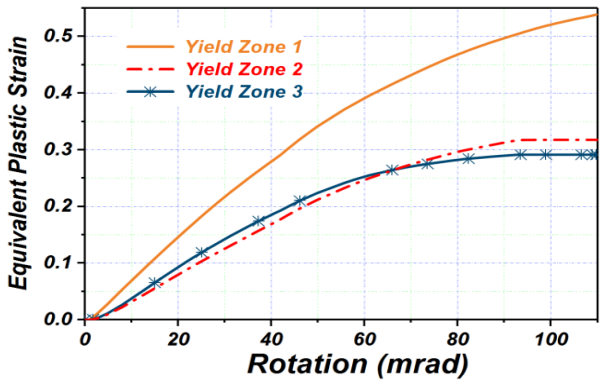

a) Evolution of equivalent plastic strain with rotation for model 35

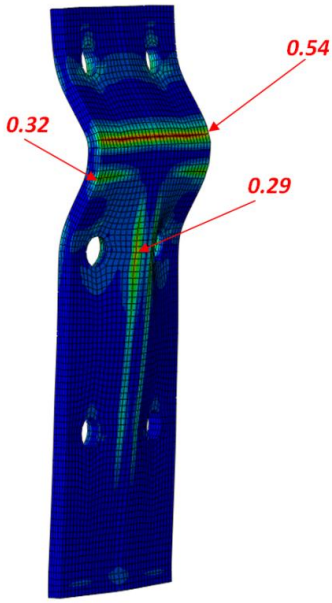

b) Yield line pattern in the end plate of model 35

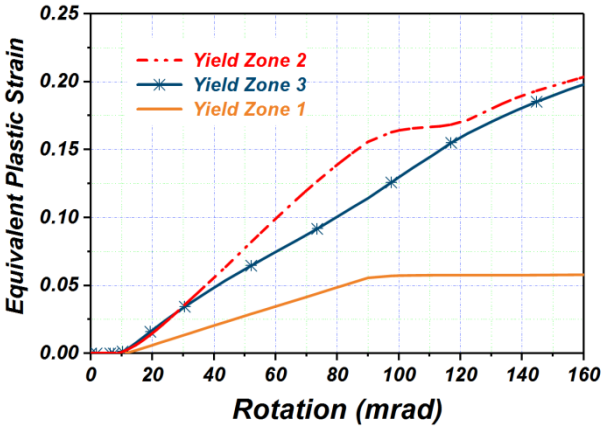

c) Evolution of equivalent plastic strain with rotation for model 67

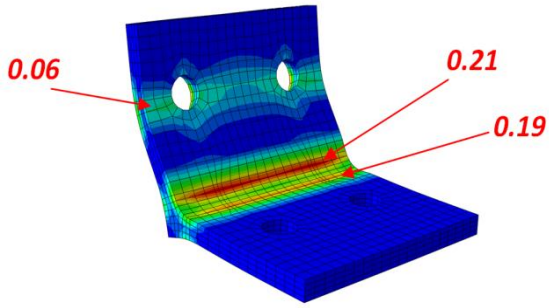

d) Yield line pattern in the top angle cleat of model 67

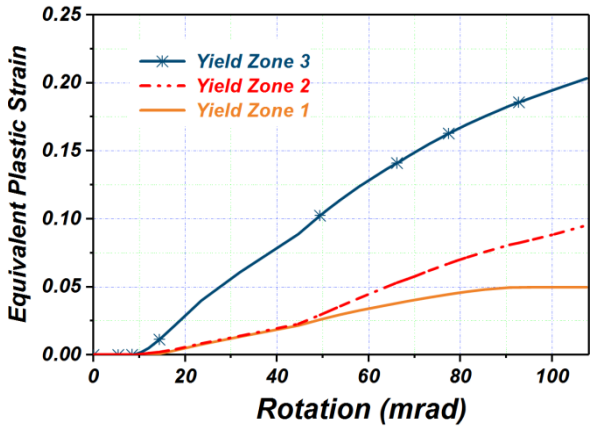

e) Evolution of equivalent plastic strain with rotation for model 75

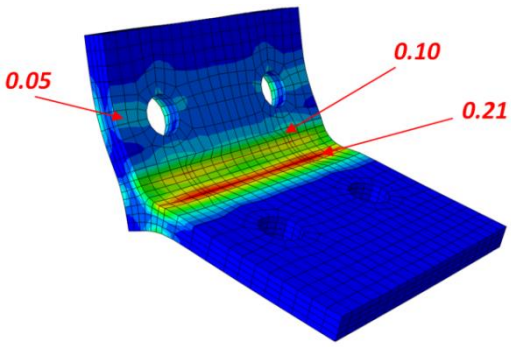

f) Yield line pattern in the top angle cleat of model 75

Fig. 7 Evolution of equivalent plastic strains and development of yield line patterns for typical joint models

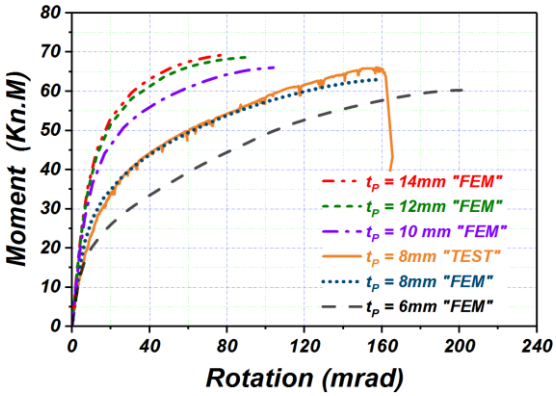

(a) *M*-Φ curves for different plate thicknesses t_p

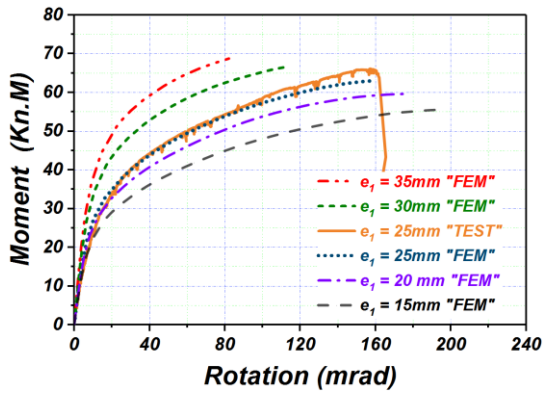

(b) *M*-Φ curves for different bolt edge distances e_1

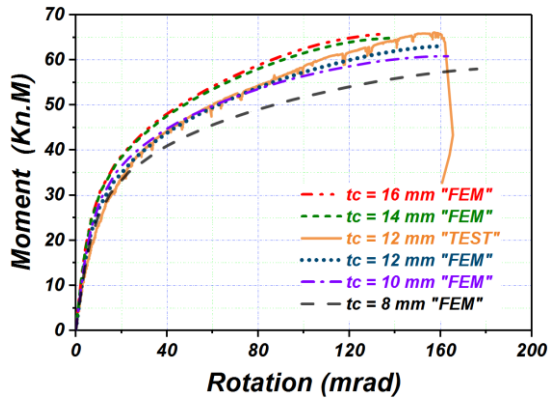

(c) *M*-Φ curves for different column flange thicknesses t_c

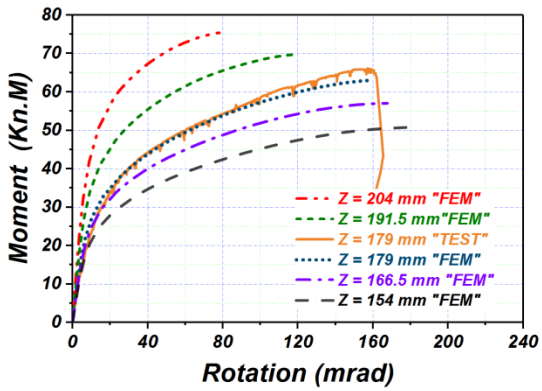

(d) *M*-Φ curves for different values of the lever arm *z*

Fig. 8 Parametric study for FEP-A connections

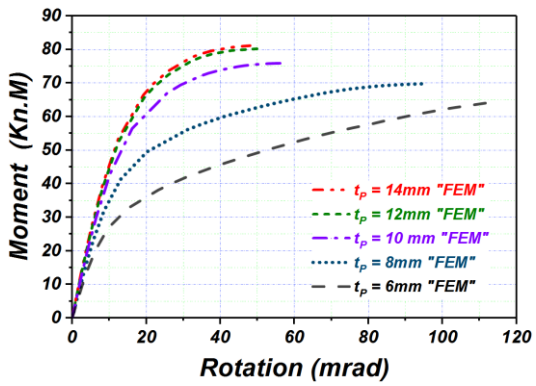

(a) *M*-Φ curves for different plate thicknesses t_p

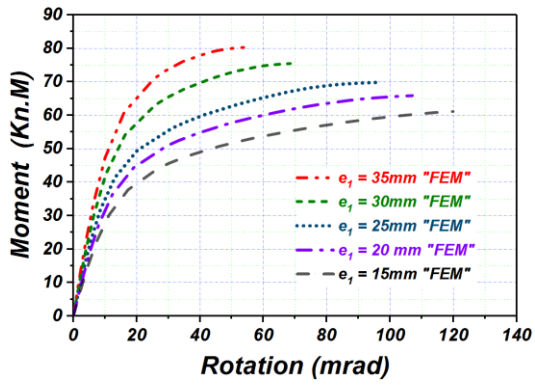

(b) *M*-Φ curves for different bolt edge distances e_1

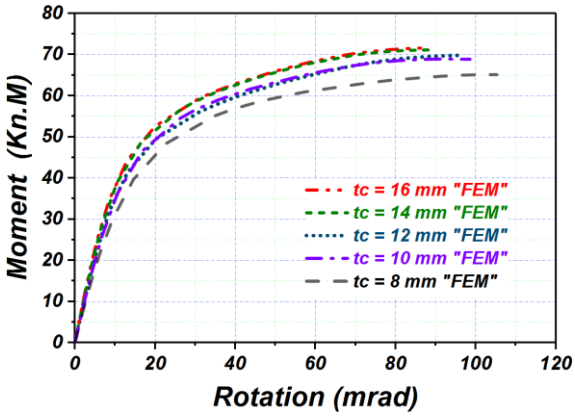

(c) *M*-Φ curves for different column flange thicknesses t_c

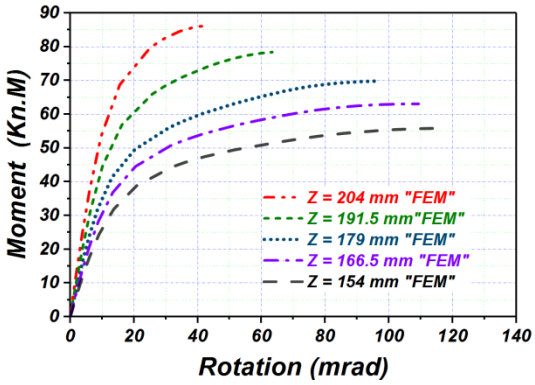

(d) *M*-Φ curves for different values of the lever arm *z*

Fig. 9 Parametric study for FEP-L connections

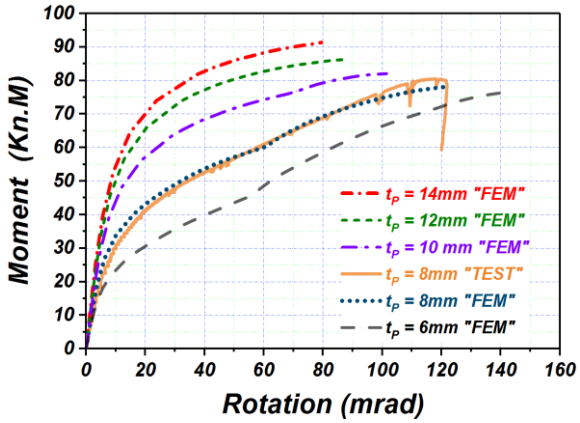

(a) *M*-Φ curves for different plate thicknesses t_p

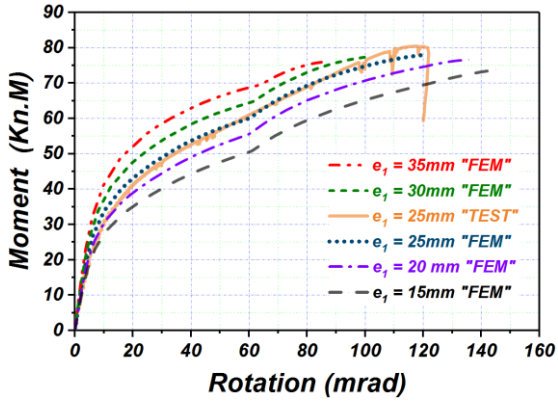

b) *M*-Φ curves for different bolt edge distances e_1

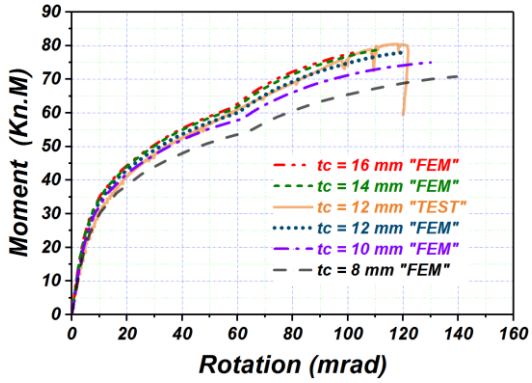

(c) *M*-Φ curves for different column flange thicknesses t_c

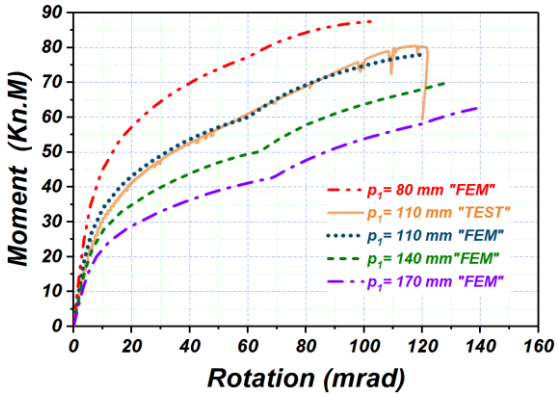

(d) *M*-Φ curves for different spacing of the first bolt row

Fig. 10 Parametric study of EEP-A connections.

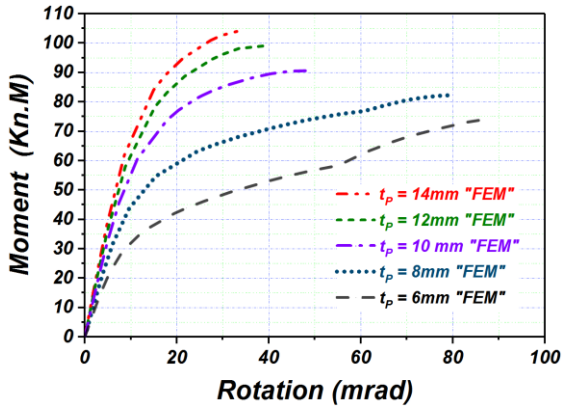

(a) *M*-Φ curves for different plate thicknesses t_p

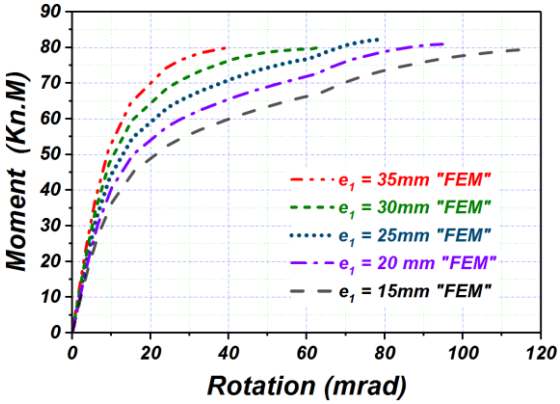

b) *M*-Φ curves for different bolt edge distances e_1

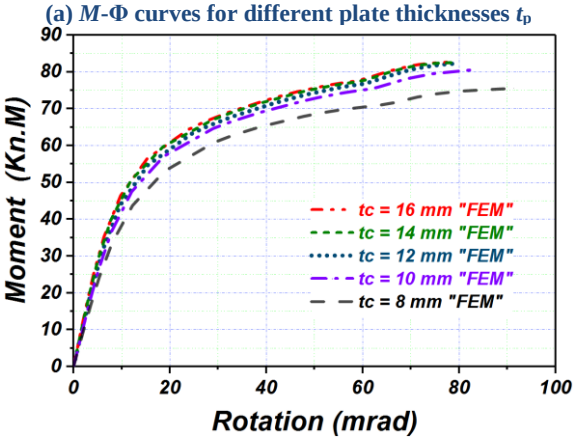

(c) *M*-Φ curves for different column flange thicknesses t_c

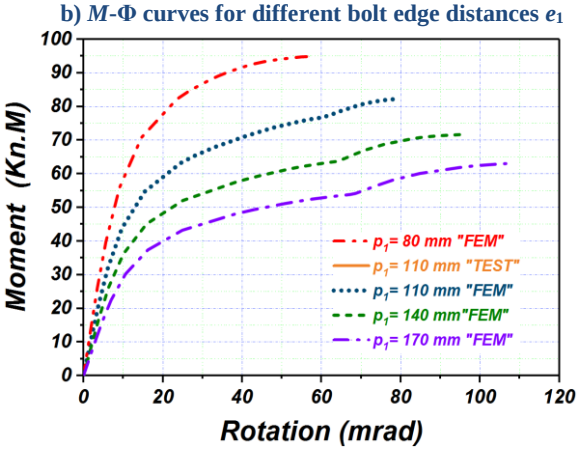

(d) *M*-Φ curves for different spacing of the first bolt row

Fig. 11 Parametric study of EEP-L connections.

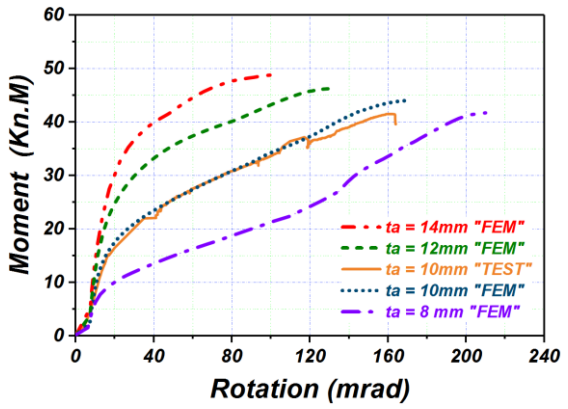

(a) M-Φ curves for different angle cleat thicknesses t_a

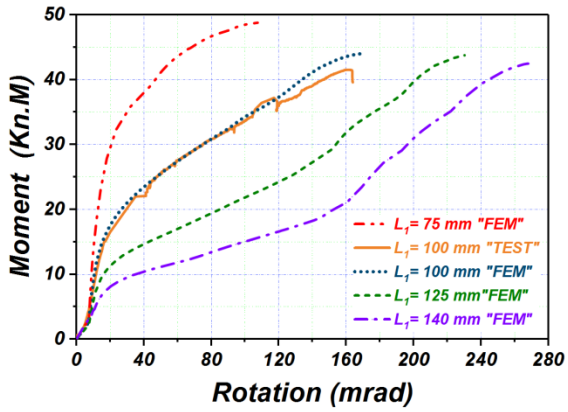

(b) M-Φ curves for different lengths L_1 of the connected angle cleats

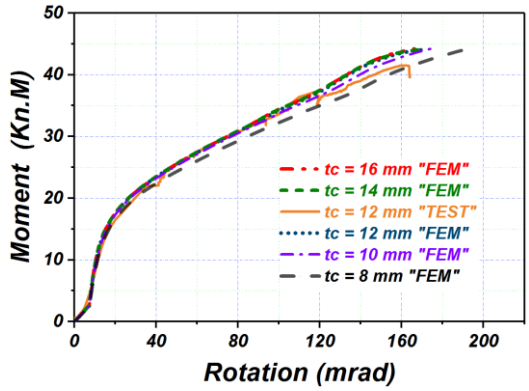

(c) M-Φ curves for different column flange thicknesses t_c

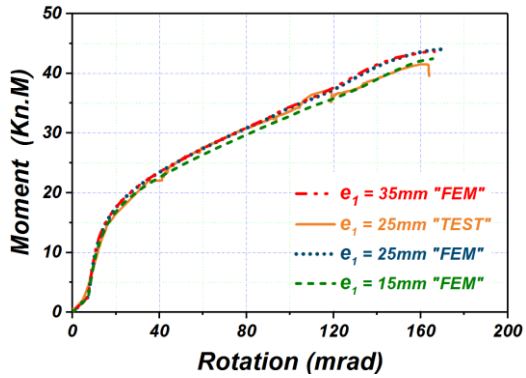

(d) M-Φ curves for different bolt edge distances e_1

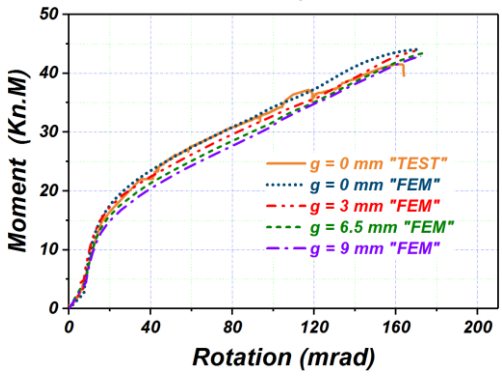

(e) M-Φ curves for different gap distances g between the beam and the column

Fig. 12 Parametric study of TSAC-10-A connections.

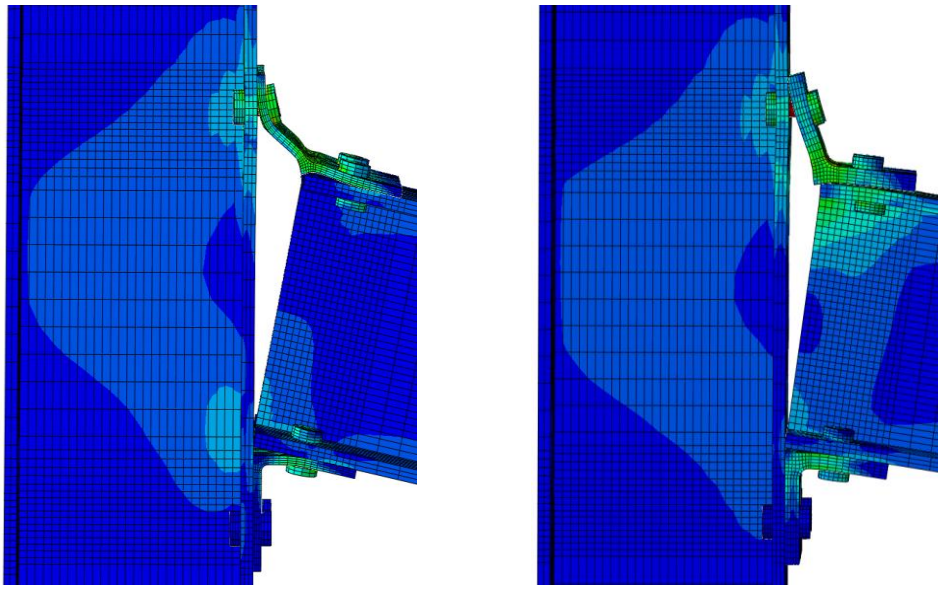

a) TSAC (ta = 8mm) b) TSAC (ta = 14 mm)

Fig. 13 Failure modes of TSAC joints with different angle thicknesses

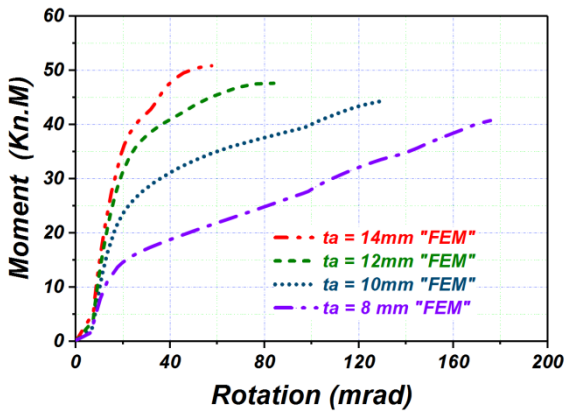

(a) M-Φ curves for different angle cleat thicknesses t_a

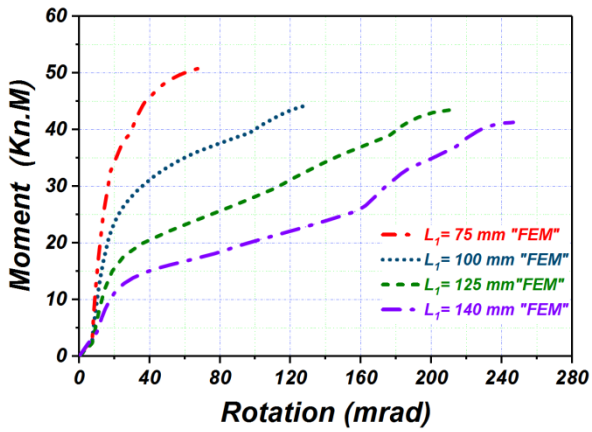

(b) M-Φ curves for different lengths L_1 of the connected angle cleats

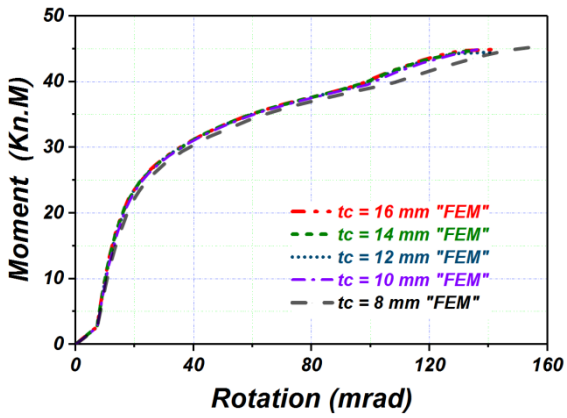

(c) M-Φ curves for different column flange thicknesses t_c

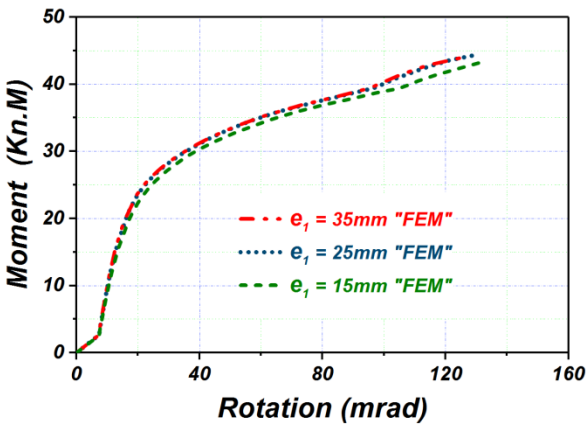

(d) M-Φ curves for different bolt edge distances e_1

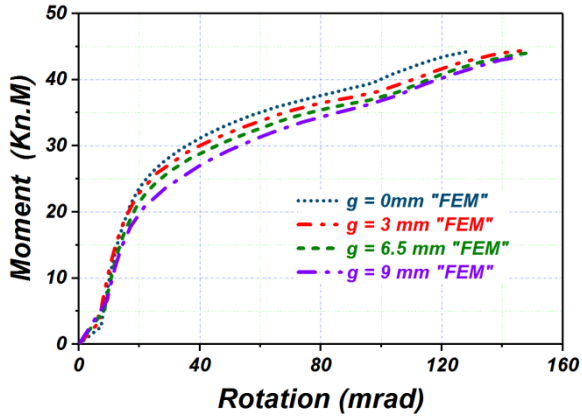

(e) M-Φ curves for different gap distances g between the beam and the column

Fig. 14 Parametric study of TSAC-10-L connections.

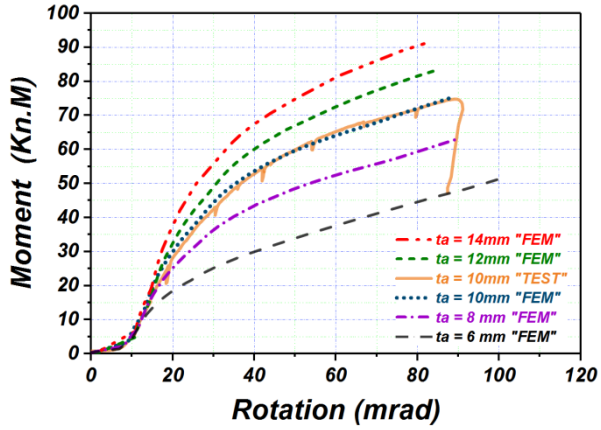

(a) M-Φ curves for different angle cleat thicknesses t_a

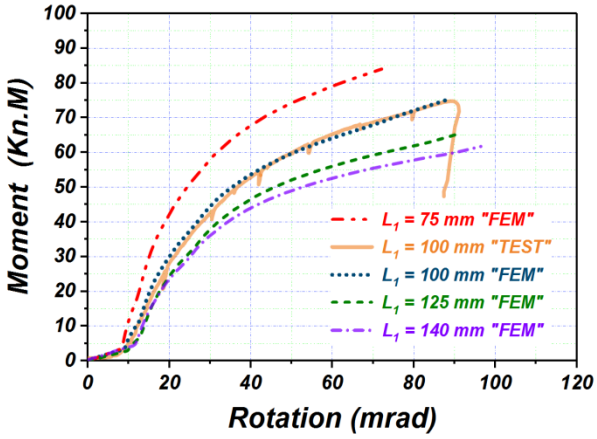

(b) M-Φ curves for different lengths L_1 of the connected angle cleats

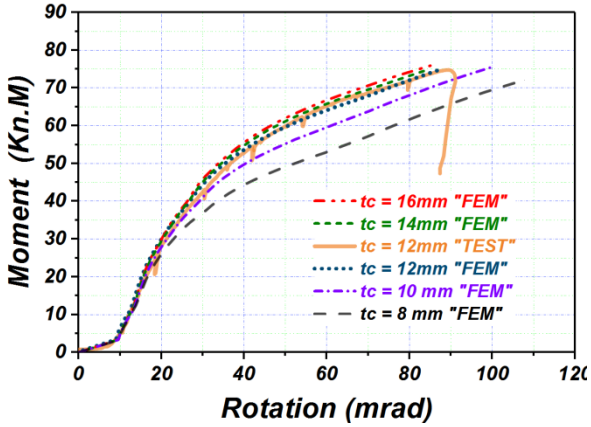

(c) M-Φ curves for different column flange thicknesses t_c

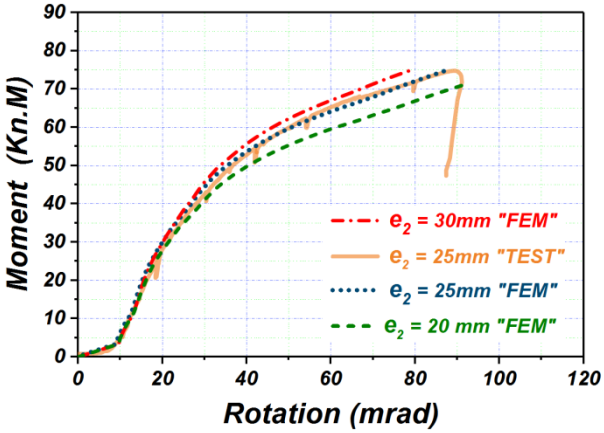

(d) M-Φ curves for different bolt edge distances e_1

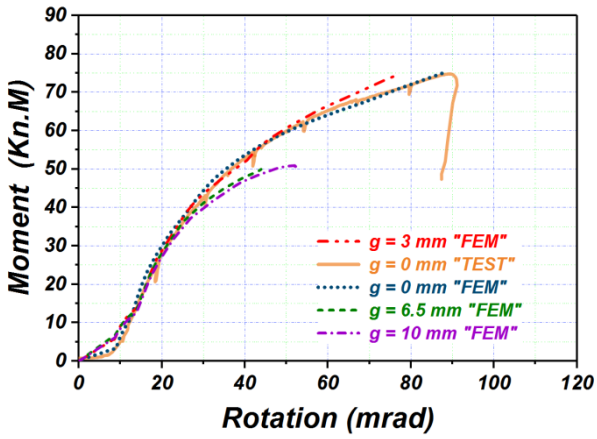

(e) M-Φ curves for different gap distances g between the beam and the column

Fig. 15 Parametric study of TSWAC-10-A connections.

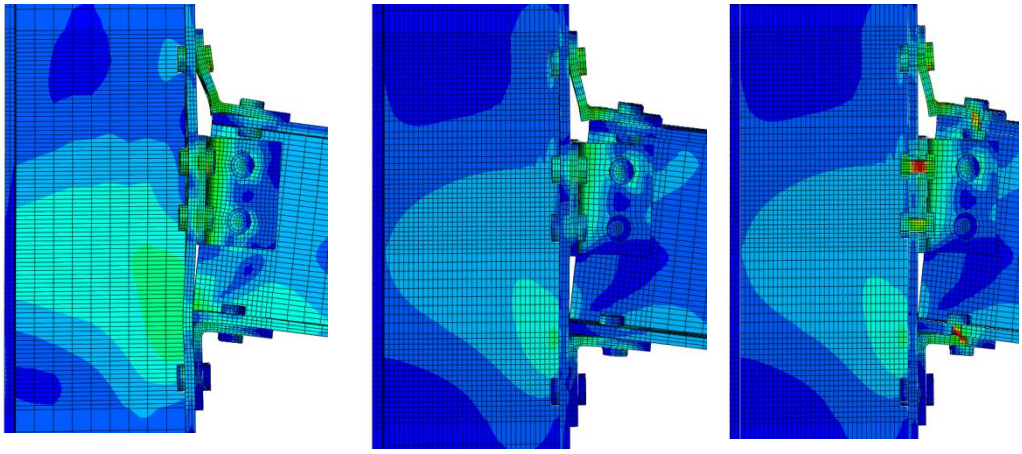

a) TSAC (g = 0 mm) **b) TSAC (g = 9 mm)** **c) TSAC (g = 9 mm)**

Fig. 16 Effect of gap g on failure mode

7 Tables

Table 1 Geometric configuration of tested specimens (symbols defined in Fig. 1)

Designation	Connection type	Distances according to Fig. 1 (mm)								
		t_c	t_p	t_a	p_1	p_2	e_1	e_2	L_1	L_2
FEP	Flush end plate	12	8	-	65	65	25	-	-	-
EEP	Extended end plate connection	12	8	-	110	100	25	-	-	-
TSAC-8	Top and seat angle cleat	12	-	8	0	0	35	-	100	-
TSAC-10	Top and seat angle cleat	12	-	10	0	0	25	-	100	-
TSWAC-8	Top, seat and web angle cleat	12	-	8	0	0	35	25	100	55
TSWAC-10	Top, seat and web angle cleat	12	-	10	0	0	25	25	100	60

Table 2 Material parameters adopted in FE modelling

Specimen	E (N/mm²)	$\sigma_{0.2}$ (N/mm²)	σ_u (N/mm²) (N/mm²)	n	m	ε_f %
I-240×120×12×10 - flange	196 500	248	630	5.20	2.37	66
I-240×120×12×10 - web	205 700	263	651	6.70	2.41	65
Angle cleat (8 mm)	197 600	280	654	12.22	2.49	55
Angle cleat (10 mm)	192 800	289	656	10.62	2.54	56
End plate	198000	282	655	12.20	2.50	54
M16 bolt (A70)	191 500	617	805	17.24	3.68	12

Table 3 Comparison of FE results with test results

Specimen	FE/Test			
	Initial stiffness $S_{j,ini}$	Plastic Moment resistance $M_{j,R}$	Maximum moment $M_{j,max}$	$\Phi_{j,u}$
FEP	0.98	0.99	1.04	0.99
EEP	0.86	0.96	1.03	0.99
TSAC-8	2.17	1.03	0.82	0.75
TSAC-10	1.50	1.06	0.94	0.95
TSWAC-8	0.80	0.94	1.16	1.31
TSWAC-10	0.96	1.03	1.00	1.04
MEAN	1.21	1.00	1.00	1.00
COV	0.44	0.05	0.11	0.18

Table 4 Summary parametric studies (geometry and results) of FEP- A

Model No.	Distances according to Fig. 1 (mm)						Initial Stiffness $S_{j,ini}$ (kN.m/mrad)			Moment Capacity $M_{j,R}$ (KN.m)			Maximum (FEM)		Yield Zone Pattern
	t_c	t_p	e_1	p_1	p_2	z	$S_{j,ini,}$ (EC3)	$S_{j,ini}$ (FEM)	EC3/ FEM	$M_{j,R}$ (EC3)	$M_{j,R}$ (FEM)	EC3/ FEM	$M_{j,u}$ (KN.m)	$\Phi_{j,u}$ (mrad)	
Model-1	12	8	25	65	65	179	5739	3995	1.44	18.6	40.5	0.46	63.0	158.5	3
Model-2	12	14	25	65	65	179	7788	5477	1.42	28.7	56.8	0.51	69.3	77.8	3
Model-3	12	12	25	65	65	179	7406	5354	1.38	28.7	54.1	0.53	68.7	89.2	3
Model-4	12	10	25	65	65	179	6786	4948	1.37	26.4	50.4	0.52	66.1	103.9	3
Model-5	12	6	25	65	65	179	4031	3562	1.13	10.5	26.7	0.39	60.3	201.1	2
Model-6	12	8	35	65	65	179	7611	5806	1.31	23.7	52.9	0.45	68.7	82.1	3
Model-7	12	8	30	65	65	179	6697	5014	1.34	20.5	48.7	0.42	66.5	111.7	3
Model-8	12	8	20	65	65	179	4743	3816	1.24	16.5	37.8	0.44	59.6	176.0	1
Model-9	12	8	15	65	65	179	3912	3353	1.17	15.3	32.5	0.47	55.6	195.1	1
Model-10	16	8	25	65	65	179	6288	4746	1.32	18.6	45.5	0.41	65.7	134.7	3
Model-11	14	8	25	65	65	179	6053	4674	1.30	18.6	44.2	0.42	64.8	136.7	3
Model-12	10	8	25	65	65	179	5290	3852	1.37	18.6	41.8	0.45	60.8	162.2	3
Model-13	8	8	25	65	65	179	4591	3650	1.26	16.1	37.5	0.43	58.0	175.9	3
Model-14	12	8	25	65	65	204	7585	6753	1.12	24.7	59	0.42	75.6	83.0	1
Model-15	12	8	25	65	65	191	6554	5387	1.22	20.5	49	0.42	69.7	120.5	1
Model-16	12	8	25	65	65	166	4956	3706	1.34	16.7	36	0.46	57.0	162.8	3
Model-17	12	8	25	65	65	154	4245	3120	1.36	15.1	31	0.49	50.7	182.4	3
MEAN									1.30			0.45			

COV									0.07			0.09			

Table 5 Summary parametric studies (geometry and results) of FEP- L

Model No.	Distances according to Fig. 1 (mm)						Initial stiffness $S_{j,ini}$ (KN.m/mrad)			Moment Capacity $M_{j.R}$ (KN.m)			Maximum (FEM)		Yield Zone Pattern
	t_c	t_p	e_1	p_1	p_2	z	$S_{j,ini,}$ (EC3)	$S_{j,ini}$ (FEM)	EC3/ FEM	$M_{j,R}$ (EC3)	$M_{j,R}$ (FEM)	EC3/ FEM	$M_{j,u}$ (KN.m)	$\Phi_{j,u}$ (mrad)	
Model-18	12	8	25	65	65	179	5838	4058	1.44	27.7	53.4	0.52	69.8	95.8	3
Model-19	12	14	25	65	65	179	7922	5622	1.41	38.9	65.2	0.60	81.1	48.0	3
Model-20	12	12	25	65	65	179	7534	5431	1.39	38.9	64.5	0.60	80.3	51.1	3
Model-21	12	10	25	65	65	179	6903	5066	1.36	32.9	59.5	0.55	75.91	56.7	3
Model-22	12	6	25	65	65	179	4100	3591	1.14	21.6	39.5	0.55	64.2	112.4	2
Model-23	12	8	35	65	65	179	7741	5625	1.38	32.2	68.4	0.47	80.3	55.1	3
Model-24	12	8	30	65	65	179	6812	5122	1.33	30.7	60.9	0.50	75.4	68.5	3
Model-25	12	8	20	65	65	179	4824	3866	1.25	24.3	47.5	0.51	65.8	107.0	1
Model-26	12	8	15	65	65	179	3979	3373	1.18	21.2	44.9	0.47	61.1	119.9	1
Model-27	16	8	25	65	65	179	6396	4861	1.32	27.7	58.5	0.47	71.6	88.4	3
Model-28	14	8	25	65	65	179	6157	4551	1.35	27.7	58.5	0.47	71.1	89.7	3
Model-29	10	8	25	65	65	179	5381	3840	1.4	27.7	54.2	0.51	68.9	98.5	3
Model-30	8	8	25	65	65	179	4670	3750	1.25	27.7	52.3	0.53	65.1	105.2	3
Model-31	12	8	25	65	65	204	7715	6759	1.14	33.3	71.1	0.47	86.1	42.2	1
Model-32	12	8	25	65	65	191.5	6666	5418	1.23	30.0	63.8	0.47	78.4	63.4	1
Model-33	12	8	25	65	65	166.5	5041	3764	1.34	25.5	50.2	0.51	63.0	109.3	3
Model-34	12	8	25	65	65	154	4318	3170	1.36	23.4	45.1	0.52	55.8	116.0	3
MEAN									1.31			0.51			
COV									0.07			0.08			

Table 6 Summary parametric studies (geometry and results) of EEP- A

Model No.	Distances according to Fig. 1 (mm)						Initial stiffness $S_{j,ini}$ (KN.m/mrad)			Moment Capacity $M_{j.R}$ (KN.m)			Maximum (FEM)		Yield Zone Pattern
	t_c	t_p	e_1	p_1	Z_1	Z_2	$S_{j,ini,}$ (EC3)	$S_{j,in}$ (FEM)	EC3/ FEM	$M_{j,R}$ (EC3)	$M_{j,R}$ (FEM)	EC3/ FEM	$M_{j,u}$ (KN.m)	$\Phi_{j,u}$ (mrad)	
Model-35	12	8	25	110	284	174	9394	5201	1.80	27.2	43.8	0.62	78.1	120.5	1
Model-36	12	14	25	110	284	174	12872	8130	1.58	44.5	75.5	0.59	91.3	79.5	1
Model-37	12	12	25	110	284	174	12189	7498	1.62	41.2	70.9	0.58	86.2	86.4	1
Model-38	12	10	25	110	284	174	11122	6715	1.65	38.4	58.5	0.66	82.1	101.4	1
Model-39	12	6	25	110	284	174	6649	4268	1.55	15.3	26.2	0.58	76.4	141.3	1
Model-40	12	8	35	110	284	174	12541	6740	1.86	35.5	55.2	0.64	75.9	84.9	1
Model-41	12	8	30	110	284	174	11005	6126	1.80	30.3	47.5	0.64	77.6	102.4	1
Model-42	12	8	20	110	284	174	7649	4973	1.54	23.3	40.2	0.58	76.6	135.6	1
Model-43	12	8	15	110	284	174	6485	4421	1.47	23.0	35.3	0.65	73.8	147.1	1
Model-44	16	8	25	110	284	174	10175	6117	1.66	27.2	44.5	0.61	78.3	104.2	1
Model-45	14	8	25	110	284	174	9839	5920	1.66	27.2	44.5	0.61	78.7	110.1	1
Model-46	10	8	25	110	284	174	8760	5168	1.69	27.2	42.2	0.64	75.0	129.9	1
Model-47	8	8	25	110	284	174	7775	4605	1.68	24.6	39.7	0.62	70.8	139.4	1
Model-48	12	8	25	80	269	189	9433	7434	1.25	30.4	59.2	0.51	87.6	104.8	1
Model-49	12	8	25	140	299	159	9109	4385	2.13	23.9	40.1	0.59	69.7	127.5	3
Model-50	12	8	25	170	314	144	9011	3425	2.70	23.2	35.5	0.65	62.6	138.8	3
MEAN									1.73			0.61			

COV									0.18			0.06			

Table 7 Summary parametric studies (geometry and results) of EEP- L

Model No.	Distances according to Fig. 1 (mm)						Initial stiffness $S_{j,ini}$ (KN.m/mrad)			Moment Capacity $M_{j.R}$ (KN.m)			Maximum (FEM)		Yield Zone Pattern
	t_c	t_p	e_1	p_1	Z_1	Z_2	$S_{j,ini,}$ (EC3)	$S_{j,ini}$ (FEM)	EC3/ FEM	$M_{j,R}$ (EC3)	$M_{j,R}$ (FEM)	EC3/ FEM	$M_{j,u}$ (KN.m)	$\Phi_{j,u}$ (mrad)	
Model-51	12	8	25	110	284	174	9555	5280	1.81	44.8	66.9	0.67	82.2	78.9	1
Model-52	12	14	25	110	284	174	13093	8245	1.59	63.8	99.8	0.64	104.0	33.1	1
Model-53	12	12	25	110	284	174	12399	7612	1.63	62.2	93.4	0.67	99.0	38.7	1
Model-54	12	10	25	110	284	174	11313	6822	1.66	57.7	83.2	0.69	90.6	47.9	1
Model-55	12	6	25	110	284	174	6763	4360	1.55	27.5	43.1	0.64	73.9	86.6	1
Model-56	12	8	35	110	284	174	12756	6839	1.87	57.8	78.8	0.73	80.1	40.5	1
Model-57	12	8	30	110	284	174	11194	6216	1.80	51.2	75.4	0.68	79.8	62.4	1
Model-58	12	8	20	110	284	174	7780	5068	1.54	38.6	65.2	0.59	80.8	94.8	1
Model-59	12	8	15	110	284	174	6596	4508	1.46	34.8	54.2	0.64	79.5	116.7	1
Model-60	16	8	25	110	284	174	10350	6226	1.66	44.8	69.2	0.65	82.6	77.9	1
Model-61	14	8	25	110	284	174	10008	6018	1.66	44.8	69.2	0.65	82.6	79.7	1
Model-62	10	8	25	110	284	174	8910	5252	1.70	44.8	65.9	0.68	80.5	82.4	1
Model-63	8	8	25	110	284	174	7908	4694	1.68	38.1	62.5	0.61	75.5	91.38	1
Model-64	12	8	25	80	269	189	9595	7572	1.27	47.3	88.4	0.54	94.9	57.0	1
Model-65	12	8	25	140	299	159	8910	4453	2.00	38.6	58.5	0.66	71.7	95.7	3
Model-66	12	8	25	170	314	144	7908	3491	2.27	34.8	52.5	0.66	63.0	106.5	3
MEAN									1.70			0.65			
COV									0.13			0.07			

Table 8 Summary parametric studies (geometry and results) of TSAC- A

Model No.	Distances according to Fig. 1 (mm)					Initial stiffness $S_{j,ini}$ (KN.m/mrad)			Moment Capacity $M_{j.R}$ (KN.m)			Maximum (FEM)		Yield Zone Pattern
	t_c	t_a	e_1	L_1	g	$S_{j,ini,}$ (EC3)	$S_{j,ini}$ (FEM)	EC3/ FEM	$M_{j,R}$ (EC3)	$M_{j,R}$ (FEM)	EC3/ FEM	$M_{j,u}$ (KN.m)	$\Phi_{j,u}$ (mrad)	
Model-67	12	10	25	100	0	2591	1011	2.56	11.1	21.8	0.51	44.1	170.3	2
Model-68	12	14	25	100	0	3544	1624	2.18	23.7	36.9	0.64	48.8	100.0	3
Model-69	12	12	25	100	0	3160	1370	2.31	17.3	31.4	0.55	46.3	131.4	2
Model-70	12	8	25	100	0	1807	571	3.17	6.6	11.7	0.56	41.7	210.0	2
Model-71	12	10	35	100	0	2596	949	2.74	11.1	22.4	0.49	43.6	166.6	2
Model-72	12	10	15	100	0	2564	954	2.69	11.1	20.1	0.55	42.4	165.5	1
Model-73	16	10	25	100	0	2634	1.024	2.57	11.1	22.1	0.50	44.2	166.1	2
Model-74	14	10	25	100	0	2616	1.004	2.61	11.1	21.4	0.52	44.0	167.8	2
Model-75	10	10	25	100	0	2551	976	2.61	11.1	21.4	0.52	44.4	176.1	2
Model-76	8	10	25	100	0	2477	929	2.67	11.1	19.8	0.56	44.1	190.8	2
Model-77	12	10	25	75	0	2879	1608	1.79	21.6	33.2	0.65	48.8	107.5	3
Model-78	12	10	25	125	0	1796	645	2.78	7.8	14.2	0.55	43.7	230.3	2
Model-79	12	10	25	140	0	1145	461	2.48	6.2	8.9	0.70	42.5	268.0	2
Model-80	12	10	25	100	3	2591	661	3.92	11.1	21.8	0.51	43.7	169.1	3
Model-81	12	10	25	100	6.5	2019	631	3.20	8.7	17.8	0.49	43.4	173.5	3

Model-82	12	10	25	100	9	2019	598	3.38	8.7	16.4	0.53	42.9	172.1	3
MEAN								2.73			0.55			
COV								0.18			0.11			

Table 9 Summary parametric studies (geometry and results) of TSAC- L

Model No.	Distances according to Fig. 1 (mm)					Initial stiffness $S_{j,ini}$ (kN.m/mrad)			Moment Capacity $M_{j.R}$ (kN.m)			Maximum (FEM)		Yield Zone Pattern
	t_c	t_a	e_1	L_1	g	$S_{j,ini,}$ (EC3)	$S_{j,ini}$ (FEM)	EC3/ FEM	$M_{j,R}$ (EC3)	$M_{j,R}$ (FEM)	EC3/ FEM	$M_{j,u}$ (KN.m)	$\Phi_{j,u}$ (mrad)	
Model-83	12	10	25	100	0	2774	1198	2.31	20.3	33.4	0.61	44.3	128.8	2
Model-84	12	14	25	100	0	3826	1821	2.10	23.7	36.5	0.65	50.8	57.6	3
Model-85	12	12	25	100	0	3404	1613	2.11	23.6	37.4	0.63	47.6	84	2
Model-86	12	8	25	100	0	1914	768	2.49	12.0	17.5	0.69	40.7	175.7	2
Model-87	12	10	35	100	0	2780	1161	2.39	20.3	33.4	0.61	44.2	127.5	2
Model-88	12	10	15	100	0	2744	1202	2.28	20.3	33.4	0.61	43.3	132.1	1
Model-89	16	10	25	100	0	2823	1241	2.27	20.3	34.0	0.60	44.9	141.8	2
Model-90	14	10	25	100	0	2803	1251	2.24	20.3	34.0	0.60	44.7	135.6	2
Model-91	10	10	25	100	0	2729	1189	2.29	20.3	33.2	0.61	44.9	136.1	2
Model-92	8	10	25	100	0	2647	1140	2.32	20.3	33.0	0.61	45.4	157.1	2
Model-93	12	10	25	75	0	3132	1828	1.71	21.6	34.2	0.63	51.0	70.4	3
Model-94	12	10	25	125	0	1885	820	2.29	14.3	19.1	0.75	43.6	213.6	2
Model-95	12	10	25	140	0	1186	580	2.04	11.4	15.9	0.72	41.3	246.6	2
Model-96	12	10	25	100	3	2774	1162	2.38	20.3	33.0	0.61	44.4	147.2	3
Model-97	12	10	25	100	6.5	2138	1126	1.89	15.9	29.4	0.54	44.1	149.9	3
Model-98	12	10	25	100	9	2138	1041	2.05	15.9	28.5	0.56	43.5	146.3	3
MEAN								2.20			0.63			
COV								0.09			0.09			

Table 10 Summary parametric studies (geometry and results) of TSWAC- A

Model No.	Distances According to Fig. 1 (mm)							Initial Stiffness $S_{j,ini}$ (kN.m/mrad)			Moment Capacity $M_{j.R}$ (kN.m)			Maximum (FEM)		Yield Zone Pattern
	t_c	t_a	e_1	e_2	L_1	L_2	g	$S_{j,ini,}$ (EC3)	$S_{j,ini}$ (FEM)	EC3/ FEM	$M_{j,R}$ (EC3)	$M_{j,R}$ (FEM)	EC3/ FEM	$M_{j,u}$ (KN.m)	$\Phi_{j,u}$ (mrad)	
Model-99	12	10	25	25	100	60	0	6140	2879	2.13	30.3	53.2	0.57	75.0	87.7	2
Model-100	12	14	25	25	100	60	0	7368	3680	2.00	55.8	67.3	0.80	91.1	81.6	2
Model-101	12	12	25	25	100	60	0	6855	3179	2.16	47.3	59.5	0.80	83.5	85.2	2
Model-102	12	8	25	25	100	60	0	4673	2390	1.96	16.7	41.6	0.41	63.4	95.5	4
Model-103	12	6	25	25	100	60	0	4673	2390	1.96	16.7	41.6	0.41	63.4	95.5	4
Model-104	12	10	25	30	100	60	0	5636	2673	2.11	26.0	53.5	0.49	75.1	79.6	4
Model-105	12	10	25	20	100	60	0	6308	2915	2.16	38.2	47.8	0.81	83.5	85.2	2
Model-106	16	10	25	25	100	60	0	6260	2673	2.34	30.3	55.97	0.55	75.9	85.1	2
Model-107	14	10	25	25	100	60	0	6174	2917	2.12	30.3	55.7	0.55	74.8	84.3	2
Model-108	10	10	25	25	100	60	0	5761	2867	2.01	30.3	45.4	0.67	75.7	100.6	2
Model-109	8	10	25	25	100	60	0	5257	2668	1.97	28.7	49.8	0.59	72.1	107.8	2
Model-110	12	10	25	25	75	60	0	5284	4009	1.32	38.8	62.9	0.63	84.0	72.1	3
Model-111	12	10	25	25	125	60	0	6455	2398	2.69	29.5	47.5	0.63	65.6	91.6	2
Model-112	12	10	25	25	140	60	0	7192	2259	3.18	30.4	43.8	0.71	61.7	96.5	2
Model-113	12	10	25	25	100	60	3	6026	2854	2.11	30.3	49.9	0.62	74.5	76.7	3

Model-114	12	10	25	25	100	60	6.5	4665	2747	1.70	19.7	39.7	0.51	49.9	43.9	3
Model-115	12	10	25	25	100	60	9	4665	2647	1.76	19.7	39.9	0.51	50.5	52.7	3
MEAN										2.11			0.61			
COV										0.19			0.19			

Table 11 Summary parametric studies (geometry and results) of TSWAC- L

Model No.	Distances according to Fig. 1 (mm)							Initial stiffness $S_{j,ini}$ (KN.m/mrad)			Moment Capacity $M_{j.R}$ (KN.m)			Maximum (FEM)		Yield Zone Pattern
	t_c	t_a	e_1	e_2	L_1	L_2	g	$S_{j,ini,}$ (EC3)	$S_{j,ini}$ (FEM)	EC3/ FEM	$M_{j,R}$ (EC3)	$M_{j,R}$ (FEM)	EC3/ FEM	$M_{j,u}$ (KN.m)	$\Phi_{j,u}$ (mrad)	
Model-116	12	10	25	25	100	60	0	6628	2952	2.25	50.18	60.8	0.83	78.7	73.1	2
Model-117	12	14	25	25	100	60	0	8136	3435	2.37	80.8	78.4	1.03	92.1	68.8	2
Model-118	12	12	25	25	100	60	0	7561	3202	2.36	66.0	71.9	0.92	87.1	70.4	2
Model-119	12	8	25	25	100	60	0	5102	2476	2.06	29.6	51.5	0.57	68.7	78.6	4
Model-120	12	6	25	25	100	60	0	5102	2476	2.06	29.6	51.5	0.57	68.7	78.6	4
Model-121	12	10	25	30	100	60	0	6175	2968	2.08	46.1	68.4	0.67	76.6	62.7	4
Model-122	12	10	25	20	100	60	0	6958	2760	2.52	52.3	56.8	0.92	81.2	81.7	2
Model-123	16	10	25	25	100	60	0	6900	3020	2.28	50.2	71.4	0.70	79.1	64.9	2
Model-124	14	10	25	25	100	60	0	6800	2922	2.33	50.2	69.4	0.72	79.0	68.7	2
Model-125	10	10	25	25	100	60	0	6319	2731	2.31	50.2	53.7	0.93	77.5	83.5	2
Model-126	8	10	25	25	100	60	0	5740	2516	2.28	49.1	49.8	0.99	71.7	87.3	2
Model-127	12	10	25	25	75	60	0	5845	3903	1.50	65.6	68.8	0.95	59.7	86.4	3
Model-128	12	10	25	25	125	60	0	7080	2376	2.98	48.4	53.1	0.91	71.3	80.4	2
Model-129	12	10	25	25	140	60	0	7903	2250	3.51	49.6	53.9	0.92	69.2	85.0	2
Model-130	12	10	25	25	100	60	3	6628	2924	2.27	50.2	53.8	0.93	75.3	57.9	3
Model-131	12	10	25	25	100	60	6.5	5069	2821	1.80	34.8	43.7	0.80	53.7	37.9	3
Model-132	12	10	25	25	100	60	9	5069	2747	1.85	34.8	43.5	0.80	53.4	43.2	3
MEAN										2.30			0.85			
COV										0.20			0.15			